Journal of Geodynamics 59–60 (2012) 133–142

Contents lists available at ScienceDirect

Journal of Geodynamics

journal homepage: http://www.elsevier.com/locate/jog

Global-scale validation of model-based load deformation of the Earth's crust from continental watermass and atmospheric pressure variations using GPS

Mathias Fritsche[a,*], Petra Döll[b], Reinhard Dietrich[a]

[a] Institut für Planetare Geodäsie, Technische Universität Dresden, 01069 Dresden, Germany
[b] Institut für Physische Geographie, Johann Wolfgang Goethe-Universität, 60054 Frankfurt am Main, Germany

ARTICLE INFO

Article history:
Received 9 December 2010
Received in revised form 4 April 2011
Accepted 18 April 2011
Available online 27 April 2011

Keywords:
Hydrological loading
Atmospheric pressure loading
Model validation
GPS processing

ABSTRACT

Temporal mass variations in the continental hydrosphere and in the atmosphere lead to changes in the gravitational potential field that are associated with load-induced deformation of the Earth's crust. Therefore, models that compute continental water storage and atmospheric pressure can be validated by measured load deformation time series. In this study, water mass variations as computed by the WaterGAP Global Hydrology Model (WGHM) and surface pressure as provided by the reanalysis product of the National Centers for Environmental Prediction describe the hydrological and atmospheric pressure loading, respectively. GPS observations from 14 years at 208 stations world-wide were reprocessed to estimate admittance factors for the associated load deformation time series in order to determine how well the model-based deformation fits to real data. We found that such site-specific scaling factors can be identified separately for water mass and air pressure loading. Regarding water storage variation as computed by WGHM, weighted global mean admittances are 0.74 ± 0.09, 0.66 ± 0.10, 0.90 ± 0.06 for the north, east and vertical component, respectively. For the dominant vertical component, there is a rather good fit to the observed displacements, and, averaged over all sites, WGHM is found to slightly overestimate temporal variations of water storage. For Europe and North America, with a dense GPS network, site-specific admittances show a good spatial coherence. Regarding regional over- or underestimation of WGHM water storage variations, they agree well with GRACE gravity field data. Globally averaged admittance estimates of pre-computed atmospheric loading displacements provided by the Goddard Geodetic VLBI Group were determined to be 0.88 ± 0.04, 0.97 ± 0.08, 1.13 ± 0.01 for the north, east and vertical, respectively. Here, a relatively large discrepancy for the dominant vertical component indicates an underestimation of corresponding loading predictions.

1. Introduction

To understand the Earth system and its temporal changes, a reliable description of geophysical processes that imply mass transport is needed. At the global scale, the water cycle comprises the most significant processes associated with mass exchange between the oceans, the continents and the atmosphere up to seasonal and interannual time scales. In addition, mass redistribution in the atmosphere, characterized by pressure changes, plays an important role. These processes are simulated by ocean circulation, hydrological and atmospheric models, respectively. To assess the validity and uncertainty of such global models, independent measurements of mass transport or the resulting temporal mass changes are required.

Temporal mass changes in the Earth system are reflected in both gravity field variations, and load deformation of the Earth's crust that is associated with the Earth's response to mass changes. While global-scale gravity field variations are observed by the Gravity Recovery and Climate Experiment (GRACE) satellite mission, space geodetic techniques such as the Global Positioning System (GPS), Very Long Baseline Interferometry (VLBI) and Satellite Laser Ranging allow the measurement of site position displacements. In particular, gravimetric and geometric measurements complement each other (e.g. Davis et al., 2004; van Dam et al., 2007).

GPS measurements are significantly affected by site displacements that are caused by crustal deformation. The application of related deformation time series for the purpose of GPS observation reduction is not yet a common standard. Rather, the effect of the residual displacements is retained in the adjusted observations and cause site coordinate estimates to show systematic variations with respect to a mean position (linear model including velocities). For instance, Dach et al. (2011) showed an improved repeatability of weekly GPS station heights between 10 and 20% on average if

* Corresponding author.
E-mail address: fritsche@ipg.geo.tu-dresden.de (M. Fritsche).

0264-3707/$ – see front matter © 2011 Elsevier Ltd. All rights reserved.
doi:10.1016/j.jog.2011.04.001

corrections for the effect of atmospheric pressure loading to GPS observations were applied.

The aim of this study is to contribute to the validation of global-scale hydrological and atmospheric models using GPS measurements. Computed changes in GPS site positions, as propagated from modelled variations in continental water storage and atmospheric pressure, are combined with GPS observations. For this purpose, the model-based mass changes, i.e. the estimates of surface mass loads, were supplemented with a gravitationally consistent ocean response (Farrel and Clark, 1976), and used to compute site displacements separately for the effects of continental water storage (hydrological loading HYDL) and atmospheric pressure (atmospheric loading ATML). Finally, the site displacement time series were used to adjust reprocessed GPS measurements of a global network with more than 200 stations (Steigenberger et al., 2006), in order to estimate site-specific and globally averaged deformation admittance factors.

2. Methodology

2.1. Modelling loads and deformation

In this study, we use time series of spatially distributed model-based surface mass load estimates related to both continental water storage and atmospheric surface pressure. However, in terms of the total load potential exerted on the Earth, the two models cannot be simply added and then propagated to changes in the Earth's geometric shape due to lacking gravitational consistency of the hydrological and atmospheric input models. In particular, total load mass is not conserved and the implied sea level does not represent an equipotential surface of the Earth's gravity field including the load (Clarke et al., 2005).

Consequently, for determining the total time-variable load T, we did not only consider the load due to continental water storage and atmospheric pressure but also due to the passive ocean load in order to enforce gravitational consistency on the input models (Blewitt and Clarke, 2003; Clarke et al., 2005). Hence, the contributions from continental water storage and atmospheric pressure form the dynamic load D which is complemented by the passive oceanic load S. All quantities are expressed in terms of the equivalent height of a column of sea water with density ρ_S. The total surface load potential T is written as a function of geographic position Ω (longitude λ, latitude ϕ)

$$T(\Omega) = D(\Omega) + S(\Omega) = \sum_{n=1}^{\infty}\sum_{m=0}^{n}\sum_{\Phi}^{\{C,S\}} T_{nm}^{\Phi} Y_{nm}^{\Phi}(\Omega) \tag{1}$$

with un-normalized spherical harmonic basis functions $Y_{nm}^{\Phi}(\Omega)$ and load coefficients T_{nm}^{Φ} of degree n and order m. $\Phi \in \{C, S\}$ identifies the expansion's cosine and sine component. As mass conservation is required, the total load's degree-zero term vanishes. In contrast, degree-zero terms of the dynamic and passive ocean load are generally non-zero ($D_{00} = -S_{00} \neq 0$) which is predominantly caused by the seasonal ocean–continent mass exchange.

The ocean's response to the dynamic load is characterized by the fact that the passive load is in hydrostatic equilibrium with the total load's gravitational potential field on time scales of several days. Therefore, $S(\Omega)$ is evaluated by the sea-level equation (cf. Dahlen, 1976; Farrel and Clark, 1976), which has the following general form

$$S(\Omega) = C(\Omega)\left[(V(\Omega) + \Delta V)g^{-1} - \delta h(\Omega)\right]. \tag{2}$$

Here, $C(\Omega)$ is the ocean-function (zero over land and unity over oceans). $V(\Omega)$ denotes the resulting change in the potential that is caused by the total load itself and the accompanied solid Earth deformation (cf. Farrell, 1972). The gravitational acceleration at the Earth surface is given by g, the constant term ΔV ensures mass conservation. The radial change in the Earth surface $\delta h(\Omega)$ is accompanied by the lateral changes in site position $\delta n(\Omega)$, $\delta e(\Omega)$ in north and east direction, respectively. The topocentric surface deformation $\mathbf{d} = [\delta n, \delta e, \delta h]'$ induced by the total load $T(\Omega)$ can be computed according to the load Love number formalism (Farrel and Clark, 1976)

$$\begin{aligned}
\delta n(\Omega) &= \frac{3\rho_S}{\rho_E}\sum_{n=1}^{\infty}\sum_{m=0}^{n}\sum_{\Phi}^{\{C,S\}} \frac{l'_n T_{nm}^{\Phi}}{2n+1}\,\partial_{\phi} Y_{nm}^{\Phi}(\Omega)\\
\delta e(\Omega) &= \frac{3\rho_S}{\rho_E}\sum_{n=1}^{\infty}\sum_{m=0}^{n}\sum_{\Phi}^{\{C,S\}} \frac{l'_n T_{nm}^{\Phi}}{2n+1}\,\frac{\partial_{\lambda} Y_{nm}^{\Phi}(\Omega)}{\cos\phi}\\
\delta h(\Omega) &= \frac{3\rho_S}{\rho_E}\sum_{n=1}^{\infty}\sum_{m=0}^{n}\sum_{\Phi}^{\{C,S\}} \frac{h'_n T_{nm}^{\Phi}}{2n+1}\,Y_{nm}^{\Phi}(\Omega).
\end{aligned} \tag{3}$$

Here, l'_n and h'_n denote the degree-dependent load Love numbers and ρ_E is the mean density of the Earth. In particular, both the deformation potential $V(\Omega)$ and the vertical surface displacement $\delta h(\Omega)$ directly depend on $D(\Omega)$ and $S(\Omega)$.

2.1.1. Hydrological loading

Time-variable HYDL was derived from temporal and spatial variations of continental water storage, i.e. of water mass on all land areas of the globe except Antarctica and Greenland, as computed by the WaterGAP Global Hydrology Model WGHM (Döll et al., 2003). WGHM computes time series of water flows and water storage. Based on monthly time series of observed precipitation (GPCC Full Data Product Version 3, Rudolf and Schneider, 2005) and other climate variables, precipitation is partitioned into evapotranspiration and runoff which is routed downstream to the ocean or to internal sinks, taking into account the effect of wetlands, lakes and man-made reservoirs. In addition, the impact of human water consumption on the total water storage is taken into account (Alcamo et al., 2003). WGHM is tuned against long-term averages of river discharge observed at 1235 gauging stations around the world (Hunger and Döll, 2008). Seasonal variations are the dominant storage change signal, with maximum values in the marginal tropics and in snow-dominated high-latitude areas. Interannual variations are associated with large-scale oscillations such as El Niño Southern Oscillation (Güntner et al., 2007).

2.1.2. Atmospheric loading

To take into account ATML, we did not process data from an atmospheric model but introduced pre-computed surface displacement values.[1] Using elastic Green's functions (numerically evaluated for a spherically symmetric, nonrotating, elastic and isotropic Earth model adopting PREM elastic parameters), Petrov and Boy (2004) calculated three-dimensional non-tidal surface displacements based on a global convolution of surface pressure field variations as provided by the National Centers for Environmental Prediction (NCEP). They showed that their computed ATML displacements are suitable for the reduction of VLBI measurements. In this study, we made use of corresponding time series that are routinely provided on a global grid ($2.5^\circ \times 2.5^\circ$) with a 6 h subdaily resolution. The inverted barometer (IB) effect is applied yielding an uniform pressure over the ocean domain. The computed displacements refer to the center of mass that includes the solid Earth and the atmosphere. Accordingly, changes in the total atmospheric mass which actually exist on annual and interannual time scales

[1] http://gemini.gsfc.nasa.gov/aplo.

(Trenberth and Smith, 2005) are omitted and thus neither contribute to the surface deformation derived nor change the total mass of the considered system (solid Earth plus atmosphere).

2.1.3. Passive ocean load

For the purpose of this study, we expanded the mass distribution provided by the WGHM model into a time series of spherical harmonic coefficients ($n_{max} = 100$) with monthly resolution and a linear fit (offset and rate) removed. Concerning the loading effect due to atmospheric pressure, we introduced the pre-computed global grid data and inverted Eq. (3) in order to expand daily displacement averages into a series of spherical harmonic coefficients ($n_{max} = 100$). Both hydrological and atmospheric model contributions were considered to constitute the dynamic load D in Eq. (1) and were used to solve for the passive ocean load S according to Eq. (2).

Based on the time-variable coefficients derived, a principal component analysis (PCA) was performed in the spectral domain for HYDL, ATML and the resulting passive ocean load. Each first eigenvector, i.e. that component contributing the largest proportion of the total variance, was evaluated in the space domain and is shown in Fig. 1 (left). In addition, Fig. 1 (right) provides the corresponding principal components describing the temporal evolution of the eigenvectors. For WGHM, the first eigenvector accounts for about 48% of the total variance and shows a strong annual variation. The spatial pattern clearly separates continental regions of large water storage variability. In particular, it can be seen, that Greenland and Antarctica are not included in the WGHM model. For the atmospheric load, the first eigenvector is less dominant as it contributes only 24% of the total variance. Again, the related principal component shows a clear annual variation. In contrast, the passive ocean load is dominated by its first eigenvector which contributes about 93% of the oceanic variance. The related principal component represents an almost uniform change in the mean sea level caused by the seasonal ocean–continent mass exchange.

With regards to Eqs. (1) and (2), S has to be computed as the ocean's response to the total load potential comprising continental water storage and atmospheric pressure in this study. However, Dahlen (1976) showed the linearity of the sea-level equation supposing a constant ocean function and Earth model (i.e. the load Love numbers here). Hence, for practical reasons, the individual passive ocean contributions were added separately.

Concerning atmospheric pressure, the adopted IB hypothesis causes only mean pressure changes to affect ocean areas (Petrov and Boy, 2004). Moreover, the sea level response to changes in the gravitational potential induced by atmospheric mass redistribution is neglected. Therefore, we obtained a non-zero solution for S when considering atmospheric pressure loading only. However, the relative magnitude of this effect is rather small. It relates to surface displacements on the order of sub-millimeter which is still within the error budget of 15% as reported for these model computations.

2.2. Geodetic concept

Accounting for ATML induced deformation, van Dam and Herring (1994) analyzed the reduction of variance of VLBI baseline length estimates. Approximately 60% of the modelled air pressure loading was found to be present in respective baseline residuals. Similar results were obtained for GPS (van Dam et al., 1994). Linear ATML regression coefficients between vertical site displacements and local pressure variations have been derived as estimable quantities from VLBI (MacMillan and Gipson, 1994) and GPS observations (Kaniuth and Vetter, 2005). Their results reveal an improved baseline length repeatability but also demonstrate the limitations of fitting local pressure variations to deformation caused by regional pressure anomalies.

Petrov and Boy (2004) validated modelled ATML displacements by estimating the admittance of site-specific pressure loading deformation time series from VLBI observations. The atmospheric pressure loading signal was expressed as the product $\alpha \cdot d$, where d is the modelled deformation signal and α the associated admittance factor. Loading displacements calculated in response to global air mass redistribution were introduced for all station coordinate components. The admittance factors were estimated from the original load-induced VLBI observations applying the commonly used least-squares adjustment (LSA).

Both ATML and HYDL affect GPS observations. Therefore, we adopt the approach of Petrov and Boy (2004) and express the combined loading signal d as the sum of the HYDL (H) and ATML (A) effect (in vector notation)

$$\mathbf{d} = \sum_{j}^{\{H,A\}} diag[\ \alpha_j^{\delta n} \quad \alpha_j^{\delta e} \quad \alpha_j^{\delta h}\ ]\,\mathbf{d}_j. \tag{4}$$

The load-induced displacements are computed for each network site according to Eq. (3). The resulting time series $\mathbf{d}_H = [\delta n_H,\ \delta e_H,\ \delta h_H]'$ and $\mathbf{d}_A = [\delta n_A,\ \delta e_A,\ \delta h_A]'$ are then applied in order to derive the admittance factors $\boldsymbol{\alpha}_H = [\alpha_H^{\delta n}, \alpha_H^{\delta e}, \alpha_H^{\delta h}]'$ and $\boldsymbol{\alpha}_A = [\alpha_A^{\delta n}, \alpha_A^{\delta e}, \alpha_A^{\delta h}]'$ (topocentric north, east and up) for each individual site. Along with other relevant (technique-specific) parameters, the factors $\boldsymbol{\alpha}$ are obtained as estimable quantities from a LSA of GPS observations $\mathbf{l}$. The corresponding observation equations are linearized according to a first-order truncated Taylor series expansion introducing approximate a priori values $\boldsymbol{\alpha}^0$ for the unknown parameters. The necessary partial derivatives $\partial\mathbf{l}/\partial\boldsymbol{\alpha}$ read as follows

$$\frac{\partial \mathbf{l}}{\partial \boldsymbol{\alpha}} = \frac{\partial \mathbf{l}}{\partial \mathbf{x}} \frac{\partial \mathbf{x}}{\partial \boldsymbol{\alpha}} = \frac{\partial \mathbf{l}}{\partial \mathbf{x}} diag[\ \mathbf{R}_1 \quad \cdots \quad \mathbf{R}_k\ ] \begin{bmatrix} \mathbf{d}_1 \\ \vdots \\ \mathbf{d}_k \end{bmatrix} \tag{5}$$

where $\mathbf{x}$ are Cartesian station coordinates. $\mathbf{R}_i$ denotes a 3×3 rotation matrix for each site ($i = 1, \ldots, k$) that relates the topocentric site displacements to the geocentric Cartesian system.

Discrepancies in both amplitude and phase between the modelled and the observed loading signal cause admittance estimates to differ from unity. Regarding the estimation of admittances, it has to be considered that the partial derivatives $\partial\mathbf{l}/\partial\boldsymbol{\alpha}$ in Eq. (5) are directly proportional to the displacements applied. Consequently, the time series $\mathbf{d}_H$ and $\mathbf{d}_A$ of the same site must not show large correlations for any component. Otherwise, the estimated admittance factors will be near rank-deficient. In particular, they are expected to be anti-correlated if both time series reveal a significant signal amplitude for the same frequency while being close in or opposite in phase. Furthermore, the accuracy of estimating $\boldsymbol{\alpha}_{H,A}$ depends on the ratio of the modelled signal with respect to the sum of the measurement noise and remaining observation residuals, e.g. originating from deficiencies in the tropospheric delay or satellite orbit modelling.

2.3. GPS observation processing

Monthly surface load coefficients derived from WGHM were added by a passive ocean load contribution that is induced only by changes in continental water storage. Then we applied Eq. (3) using degree-1 load Love numbers in the center of mass (CM) reference frame (Blewitt, 2003) along with linear interpolation in order to obtain daily three-dimensional displacements $\mathbf{d}_H$ for the globally distributed network sites. Concerning ATML $\mathbf{d}_A$, the grid values were interpolated to the individual site position. Subsequent 6-h samples were linearly interpolated to the GPS

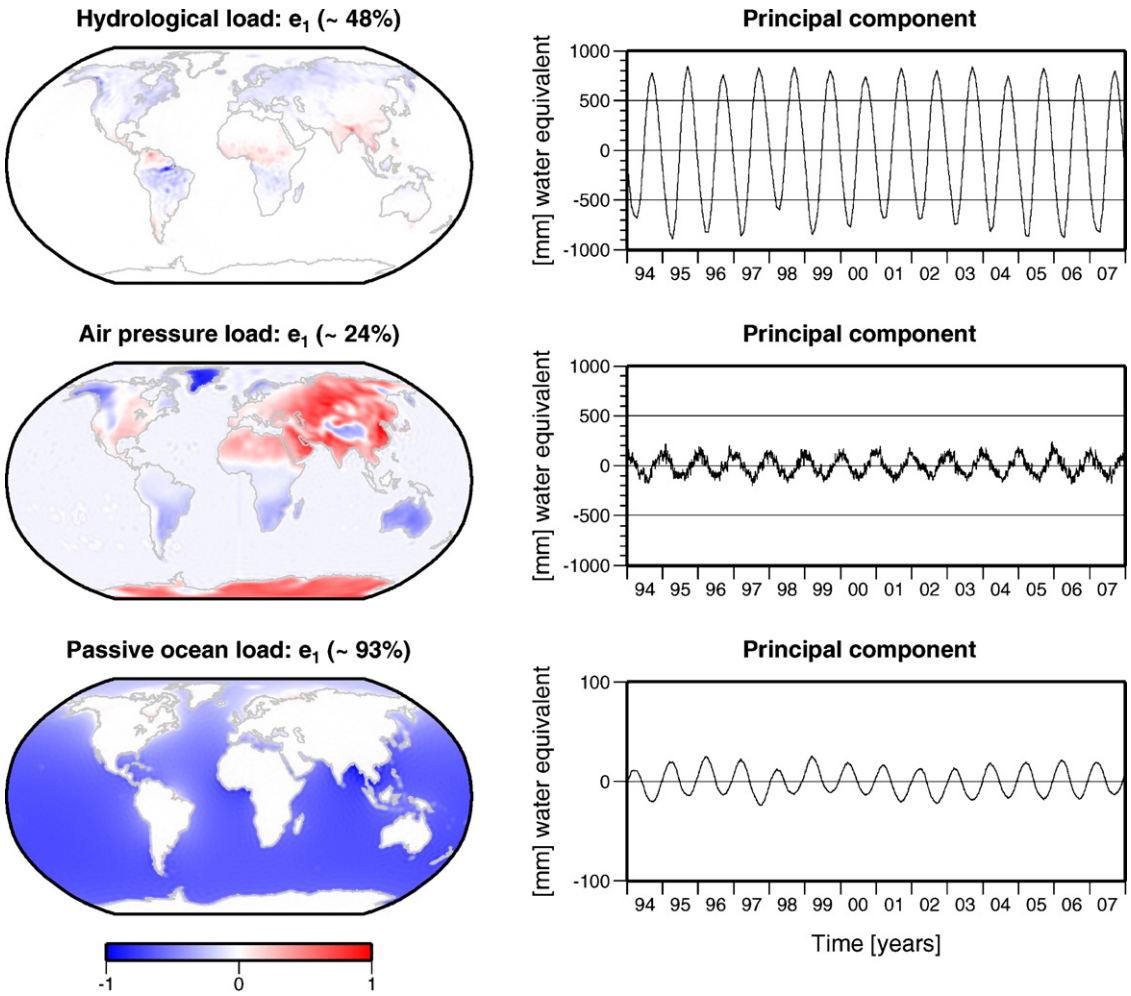

Fig. 1. Principle component analysis: components contributing the largest variance (first eigenvector $\mathbf{e}_1$ left column, proportion of total variance explained in brackets) for the continental water storage, air pressure and passive ocean load (from top to down) as well as time series of related principle components (right column).

observation epoch. In addition, we accounted for the effect of the S_1- and S_2-atmospheric tides (Ponte and Ray, 2002) and added the passive ocean load contribution from the atmosphere as daily average.

We modified the Bernese GPS Software version 5.0 (Dach et al., 2007) to set up site-specific admittance factors as estimable parameters according to Eq. (5) for 208 stations world-wide. Preprocessed double differenced phase observations as a result from a reprocessing effort of Technische Universität Dresden and Technische Universität München were used to derive global GPS solutions by producing daily normal equation (NEQ) systems for the time interval 1994.0–2008.0. According to common practice, we introduced a priori admittance factors $\boldsymbol{\alpha}^0 = 1$ for the computation of both the approximate observations and the partial derivatives. In consequence, the adjusted observations contain the corrections due to HYDL and ATML deformation which has been shown to be the most appropriate way to account for tidal and non-tidal ATML displacements (Tregoning and van Dam, 2005). In general, the final admittance factors are given according to $\boldsymbol{\alpha} = \boldsymbol{\alpha}^0 + \Delta\boldsymbol{\alpha}$.

With regards to the GPS observation modelling, neglected load-induced crustal deformation can partially be compensated by a mismodelling of the zenith hydrostatic delay (ZHD) (cf. Tregoning and Herring, 2006; Steigenberger et al., 2009). Similarly, this holds for the HYDL and ATML effect (Tregoning and Watson, 2009). Therefore, estimated admittance factors are systematically affected by deficiencies in the representation of the tropospheric delay. Consequently, we introduced the ZHDs derived from a global grid representation[2] and applied the corresponding hydrostatic and wet Vienna Mapping Functions VMF1 (Boehm et al., 2006) for the estimation of 2-h tropospheric zenith delays.

The resulting daily NEQ systems span the time interval 1994.0–2008.0 and were combined to explicitly solve for station coordinates (and velocities), Earth rotation parameters (pole coordinates) and constant site-specific admittance factors in a common adjustment. In case of a GPS–GPS-collocation (more than one receiver occupied at the same station, 29 collocations in total) the corresponding admittance parameters were combined on the NEQ level before the generation of the solution. To invert the rank-deficient accumulated normal equation matrix, additional no-net-rotation conditions were applied with respect to the station network orientation and the respective orientation rate (cf. Rülke et al., 2008; Fritsche et al., 2009).

3. Results

3.1. Separability of loading signals

Our principal component analysis (Fig. 1) shows that the HYDL signal is dominated by an annual variation, while the ATML signal is characterized by an annual variation and further relevant

[2] http://ggosatm.hg.tuwien.ac.at/DELAY.

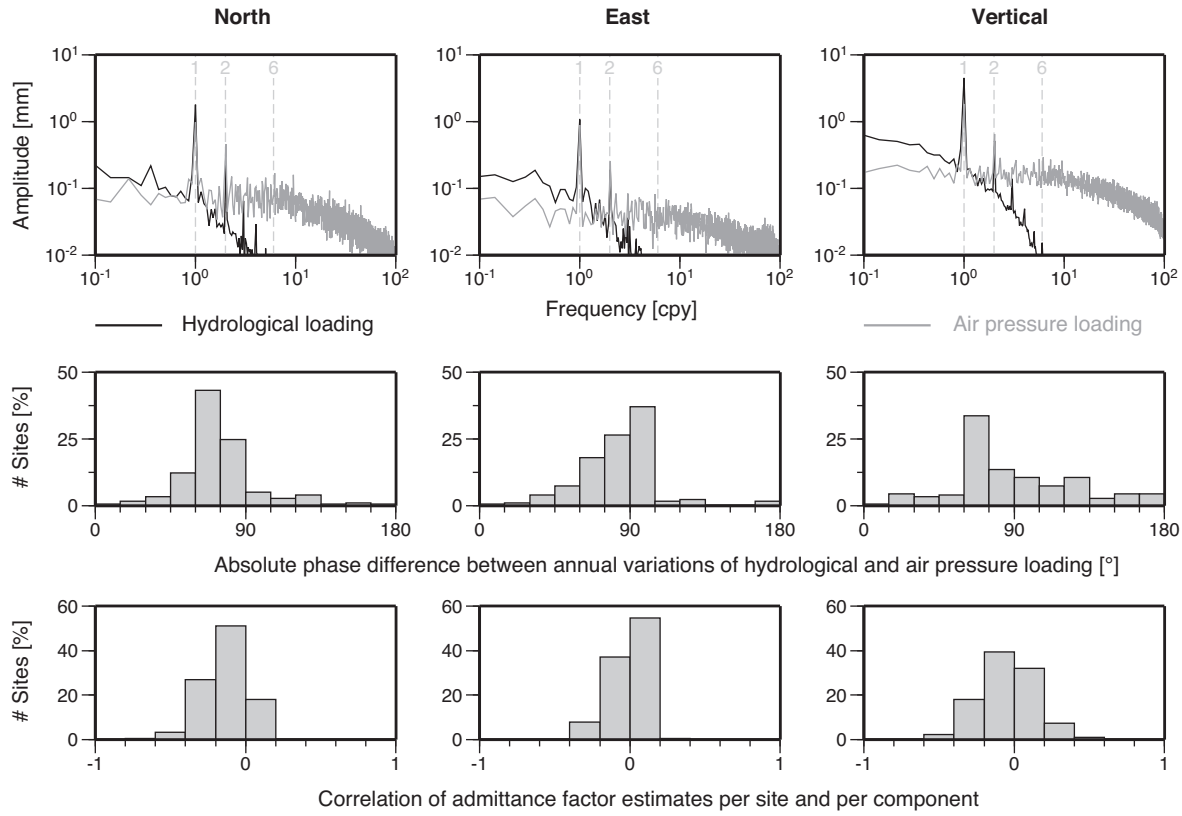

Fig. 2. Separability of hydrological (HYDL) and atmospheric pressure (ATML) loading deformation time series. Amplitudes of Fourier spectra averaged over all sites (top, multiples of annual harmonic highlighted), histograms of the phase difference between the annual variations of HYDL and ATML (center), and histograms of error-correlation coefficients between the admittance factor estimates of HYDL and ATML time series (bottom).

constituents at subannual frequencies. This confirms conclusions by Schmidt et al. (2008) regarding HYDL (obtained from the analysis of GRACE and hydrological model data), and of Petrov and Boy (2004) regarding ATML. To test whether modelled HYDL and ATML displacement time series are largely uncorrelated such that α_H and α_A could be estimated separately, we applied fast Fourier transformations to each displacement time series. The top panel of Fig. 2 shows the mean amplitudes of Fourier spectra that result from averaging over all sites. With the exception of an annual variation, both types of deformation time series considerably differ in the spectral domain thus ensuring the partial derivatives $\partial\mathbf{l}/\partial\boldsymbol{\alpha}_{H,A}$ to show less correlations with an increased observation interval. However, for both HYDL and ATML displacements the annual fraction is most important and therefore dominates the derivatives. Accordingly, we computed the phase difference between the HYDL and ATML annual fractions for each site (Fig. 2 center). For the majority of sites, the modelled HYDL and ATML annual variations are neither in nor opposite in phase, a fact that helps to discriminate both sources of deformation. In fact, the relatively small correlations between the estimated site-specific admittance factors α_H and α_A per component as extracted from the error-covariance matrix (Fig. 2 bottom) confirm the possibility of their simultaneous estimation. Therefore, our set of GPS data can be used for a joint validation of both hydrological and atmospheric model.

3.2. Site-specific deformation admittance

Although WGHM is defined for continental regions only, the global convolution of respective mass redistribution causes surface deformation for ocean sites, too. The top panel of Fig. 3 illustrates the root mean square (RMS) of the time series of HYDL deformation from 1994.0 to 2008.0. Only a small number of sites is located in regions where the total loading effect reaches its largest amplitudes (e.g. close to the Amazon basin or Siberia). However, for 60% of the 208 GPS sites, the RMS of the total displacement is larger than 3 mm, with dominant contributions from the vertical component. Estimated site-specific admittance factors related to HYDL are shown in the bottom panel of Fig. 3. The closer to 1 the deformation admittance values are, the better WGHM can explain parts of observed GPS site displacements. If the admittance is smaller than 1, WGHM overestimates the site displacement and thus continental water mass variations. Regarding the north and east components, 37% and 30% of the sites, respectively, show a factor of $0.8 \leq \alpha_H \leq 1.2$. For the dominant vertical displacement component, 47% of the sites are within this range. These sites are predominantly located in Europe and North America but many ocean sites are included, too.

Surface deformation due to ATML shows a signal that is comparable in amplitude to HYDL, but has a different spatial pattern (Fig. 4 top). For 58% of all sites, the RMS of the total displacement time series is larger than 3 mm. Surprisingly, a very good agreement between the model and real observations can be deduced from the north component. Here, 78% of all sites show an admittance factor of $0.8 \leq \alpha_A \leq 1.2$. In comparison, with 58% and 56%, the agreement is somewhat worse for the east and vertical component, respectively. Like for HYDL, best values are obtained for sites in Europe and North America (Fig. 4 bottom).

As stated in Section 2.2, the accuracy of the admittance estimation depends on the signal to noise ratio, i.e. the amplitude of the deformation. Fig. 5 shows the obtained site-specific admittance factors as a function of the RMS of associated HYDL and ATML displacement time series (top and center). In comparison to ATML admittance factors, HYDL admittance factors reveal a larger scatter with respect to the average for all three components. For both HYDL and ATML, the vertical component clearly shows that the

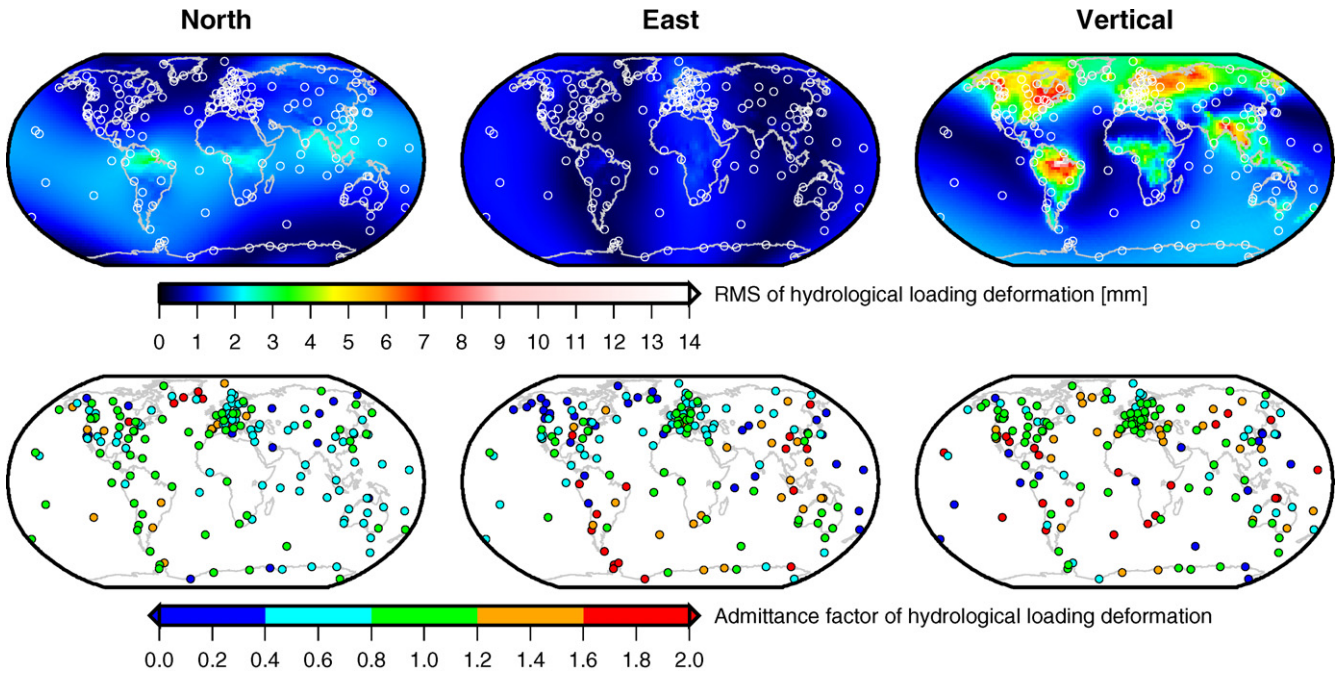

Fig. 3. Root mean square (RMS) of modelled surface displacements due to continental water storage variations as computed by the WaterGAP Global Hydrological Model (Döll et al., 2003) for the time period 1994.0–2008.0 (top), and estimated site-specific admittance factors of associated deformation time series (bottom). Circles depict the GPS sites used in this study.

scatter of computed admittances decreases with increasing RMS of the associated deformation time series. Moreover, admittance factors corresponding to larger load deformation converge to the average value. Furthermore, we generated a separate solution in which the admittance factors were estimated for the combined loading effect (Fig. 5 bottom). A general feature that can be observed is the increased RMS of the combined loading time series for all three components. As the annual HYDL and ATML variations are not out of phase (Fig. 2 bottom) they do not cancel each other out. Rather, individual contributions tend to amplify the total effect.

3.3. Globally averaged deformation admittance

In order to assess the overall performance of the load-induced displacement time series and thus of the geophysical models, we determined the globally averaged deformation admittance as a weighted mean of the site-specific values. Corresponding results were obtained by the combination of site-specific factors at the NEQ level. Since the partial derivatives $\partial \mathbf{l}/\partial \boldsymbol{\alpha}$ are directly proportional to the modelled signal d, the global admittance factors adequately account for the individual contributions. We generated four

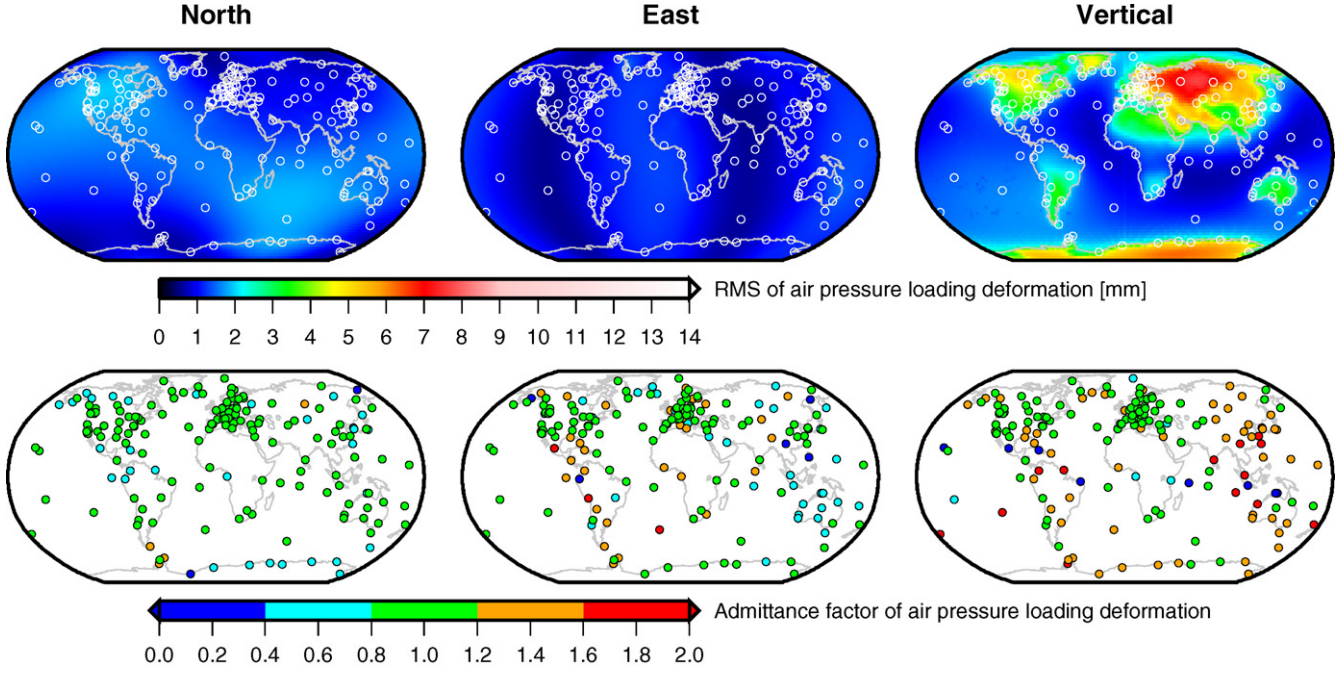

Fig. 4. Root mean square (RMS) of modelled surface displacements due to atmospheric pressure loading (computed by Petrov and Boy, 2004) for the time period 1994.0–2008.0 (top), and estimated site-specific admittance factors of associated deformation time series (bottom). Circles depict the GPS sites used in this study.

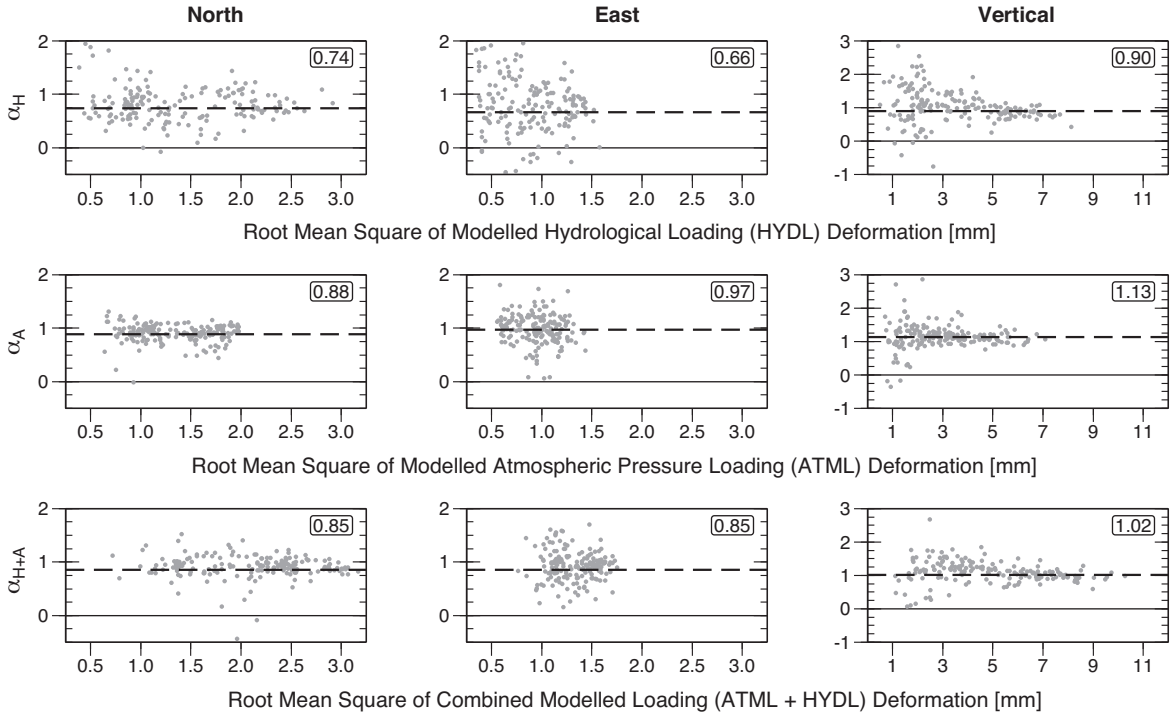

Fig. 5. Deformation admittance factors estimated from 14 years of GPS measurements. Best fit is obtained between modelled and observed GPS site displacements if admittance equals 1. Site-specific factors (dots) for hydrological (HYDL, top), atmospheric (ATML, middle) and combined (HYDL + ATML, bottom) deformation time series. HYDL and ATML specific results stem from a common solution. Site-specific estimates are plotted against the RMS of corresponding displacement time series (see top of Figs. 3 and 4). Dashed lines and boxed numbers refer to globally averaged values.

individual solutions in which the HYDL and ATML loading corrections were applied differently. The results are summarized in Table 1 and depicted by dashed lines in Fig. 5.

In solution [1] we accounted for both model corrections, while the admittance was determined for both fractions separately. The averaged HYDL admittance (weighted by the deformation signal amplitude, see above) was estimated to be 0.74 for the north, 0.66 for the east and 0.90 for the vertical component (Fig. 5 top). Notably larger values are obtained for the ATML signal, with 0.88, 0.97 and 1.13, respectively (Fig. 5 center). When compared to the HYDL model, the horizontal ATML components show a better fit to the GPS measurements as the admittances are closer to 1. In addition, standard deviations of the site-specific admittance factors with respect to the global averages are larger for HYDL than for ATML (Table 1 and Fig. 5). In general, admittance factors below 1 indicate that the geophysical model overestimates the actual load contributions present in the measurements. The ATML vertical component is the only one that appears to be underestimated.

Next we stacked the parameters α_H and α_A from solution [1] prior to the NEQ inversion in order to solve for one common factor, i.e. setting $\alpha_H = \alpha_A$. In consequence, the resulting admittance factors of solution [2] refer to the combined loading signal (HYDL plus ATML). Admittance factors of solution [2] are between the values for ATML and HYDL obtained for solution [1] because both loading models show similar RMS (Fig. 5 bottom, cf. top of Figs. 3 and 4). In two further solutions we either took into account only HYDL (solution [3]) or ATML (solution [4]). When accounting for the deformation caused by only one source, the admittance estimates show small deviations from those obtained in the reference solution [1]. The largest difference appears in case of the north ATML component, while differences for the dominant vertical components are negligible (Table 1). Hence, our results confirm the feasibility of a comparison of admittance estimates that stem from other analyses in which either the effect from HYDL or ATML has been considered.

Furthermore, solution [4] is comparable to the results obtained by Petrov and Boy (2004) who accounted only for the effect induced by ATML but not by HYDL. With regards to the global ATML admittance, they obtained 1.00 and 0.95 for the horizontal and vertical component, respectively, as compared to our solution [4*], with 0.86 and 1.14, respectively. Observations from VLBI seem to better fit to the same a priori ATML model than GPS observations do. The improved performance in the study of Petrov and Boy (2004) may

Table 1
Globally averaged deformation admittance factors α from 14 years of GPS measurements.

Solution number	Correction for HYDL/ATML	α_{North}		α_{East}		α_{Up}	
		HYDL	ATML	HYDL	ATML	HYDL	ATML
1	+/+	0.74 ± 0.09	0.88 ± 0.04	0.66 ± 0.10	0.97 ± 0.03	0.90 ± 0.06	1.13 ± 0.01
2	+/+	0.86 ± 0.03		0.86 ± 0.04		1.02 ± 0.03	
3	+/−	0.69 ± 0.09		0.66 ± 0.11		0.89 ± 0.06	
4	−/+		0.80 ± 0.04		0.92 ± 0.03		1.14 ± 0.02
4*	−/+		0.86 ± 0.03				1.14 ± 0.02
Petrov and Boy (2004)			1.00 ± 0.07				0.95 ± 0.02

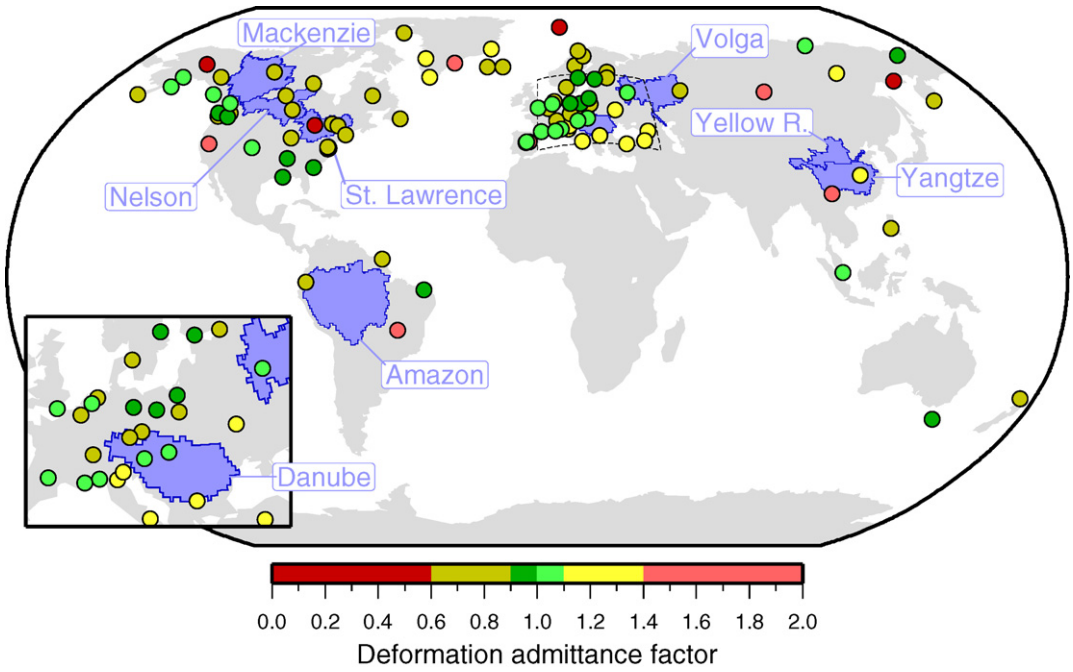

Fig. 6. Deformation admittance factors for the vertical displacement component that is due to continental water storage variations (HYDL). Only those 92 sites are shown where the displacement time series have a root mean square larger than 3 mm (cf. Fig. 3 top). The subfigure shows a zoom for Europe. Selected river basins are highlighted in blue.

be explained not only by the smaller number of contributing VLBI sites but also by the exclusion of site-specific admittance factors that exceeded a certain error limit. In contrast, all GPS sites were taken into account in our analysis.

4. Discussion

We made use of GPS observations to assess the validity of surface deformation that was derived from modelled continental water storage and atmospheric pressure variations. Accordingly, we have to take into account two major error sources in the computation of the site displacements (Eq. (3)): (1) Errors that occur when water storage and pressure variations are translated into site displacements, in particular errors in the load Love numbers, and (2) errors in modelling water storage and air pressure variations. The load Love numbers applied in this study are valid for a spherically symmetric, nonrotating, elastic and isotropic Earth model. We applied the same Love number values for the computation of the effect due to hydrological and atmospheric pressure loading. The transition to a more realistic Earth model including anisotropy and anelasticity has only a small effect which is typically of the order of 1–3% (Pagiatakis, 1990). As the globally averaged vertical admittance estimates indicate much larger total deviations (cf. Table 1), we conclude that the major reason for the discrepancy between measured and modelled GPS site displacements are errors in modelled continental water storage and air pressure variations.

4.1. Continental water storage variations

Modelling of continental water storage changes by WGHM appears to suffer from larger uncertainties than modelling of air pressure by NCEP. One reason may be that the implied NCEP data set is a reanalysis product that was obtained by assimilating measured air pressure into an atmospheric model, i.e. the modelled air pressure is continuously updated throughout the whole simulation based on measurements. In WGHM, on the other hand, only one model parameter is adjusted that is then assumed to be constant throughout the whole simulation period.

As the accuracy of the deformation admittance factors depends on the signal to noise ratio, we concentrate on the results obtained for the vertical component. Assuming a GPS carrier phase measurement error of 2 mm, we consider in Fig. 6 only those 92 GPS sites where the time series for the vertical displacement shows an RMS larger than 3 mm. 32% of those sites have an admittance between 0.9 and 1.1. The weighted mean admittance for the selected stations is 0.88, very similar to the mean admittance of 0.90 referring to all 208 stations. The unweighted average is 0.95 for the selected stations, as compared to 0.98 for all stations. This reflects that stations with smaller displacements tend to have larger admittance factors (cf. Fig. 5). Furthermore, these mean admittance estimates indicate that on average, WGHM slightly overestimates water storage variations.

Site-specific admittance estimates allow assessing the geographic differences of the uncertainty of WGHM results. For a quantitative evaluation of these point values, it has to be considered that the implied load-induced deformation depends on both the magnitude of the water storage variation and its spherical distance from the site. The relative influence of a load falls off with increasing distance. Roughly estimated, the vertical displacement caused by a load at a distance of 10 km is reduced to 5% and 0.1% if the same load is located at a distance of 100 km and 1000 km, respectively.

Over Europe and North America, with a dense GPS network, we find good agreement of observed and modelled vertical GPS displacements (Fig. 6). There, many admittance values are between 0.9 and 1.1 and, in addition, show a good spatial coherence. In Northern Europe, WGHM tends to overestimate water storage variations, while in Western Europe and particularly in Southeastern Europe including parts of Western Asia WGHM appears to underestimate water storage variations. Like in snow-dominated Northern Europe, an overestimation can also be diagnosed for most of Canada. For other continental regions the model validation is less reliable either

due to a sparse GPS station network or model predictions with a smaller signal magnitude.

A comparison of water storage variations as modelled by WGHM with seasonal water storage variations as observed by the GRACE satellites showed that WGHM significantly underestimates storage variations in 17 out of the 28 largest river basins world-wide, while there is a significant overestimation for 6 river basins (Werth and Güntner, 2010). This finding is not inconsistent with the globally averaged vertical admittance of 0.9 obtained in this study, because the geographical distribution of the considered GPS sites is highly heterogeneous, with a heavy bias towards Europe and North America. The GPS results for Europe and North America are mostly consistent with the findings of Werth and Güntner (2010). The only 6 river basins with a significant overestimation of water storage variations as compared to GRACE include the Mackenzie, Nelson and St. Lawrence in North America, for which the GPS sites located within the basins also indicate an overestimation (Fig. 6). For the Volga basin, the overestimation cannot be confirmed as there are only two GPS stations close to the basin boundaries. WGHM storage variations in the Danube basin in Southeastern Europe are underestimated compared to both GRACE and GPS. However, it is difficult to compare results for the very few GPS sites associated with large displacements outside of Europe and North America to GRACE results. The other 2 basins in which WGHM appears to overestimate water storage variations are the Yangtze and Yellow River basins in China (Fig. 6). In the Yellow River basin, no GPS site could be evaluated. The admittance of the GPS site within the Yangtze basin indicates an overestimation which corresponds to the GRACE results. For the Amazon, where WGHM strongly underestimates seasonal water storage variations as compared to GRACE, the only GPS site, which, however, is located at the very upstream end of the basin, also indicates an overestimation.

4.2. Atmospheric mass variations

Regarding our global admittance averages, an amplification of the vertical ATML by 13% (cf. Table 1) is necessary in order to fit best to our GPS observations. This scaling factor might be explained by the special choice of the degree-0 and degree-1 load Love numbers[3] made by Petrov and Boy (2004). Therefore, they did not take into account the variation of the total atmospheric mass in the displacement computation procedure, i.e. global mean pressure variations were neglected. However, Trenberth and Smith (2005) reported changes in the total atmospheric pressure with a predominant annual amplitude of 0.29 hPa mainly due to changes in the water vapor content of the atmosphere. In terms of Eq. (1), this relates to a pure degree-0 surface load with an amplitude of 3.0 mm water equivalent. Supplementing that load portion with the corresponding ocean's response, we find maximum surface displacements of 0.5 mm in radial and 0.3 mm in horizontal direction with respect to the CM frame. Thus, the neglect of this load deformation portion likely contributes to the discrepancies of the averaged admittance factors from unity.

In addition, different from the nature of VLBI observations, the orbiting GPS satellites are capable to sense CM. Therefore, the GPS measurements are sensitive to additional fractions of the total load deformation which might be a further explanation for the apparently better agreement obtained for VLBI.

Dach et al. (2011) validated the same ATML model also by means of estimating scaling factors for load deformation time series using GPS but did not account for HYDL. Moreover, no globally averaged

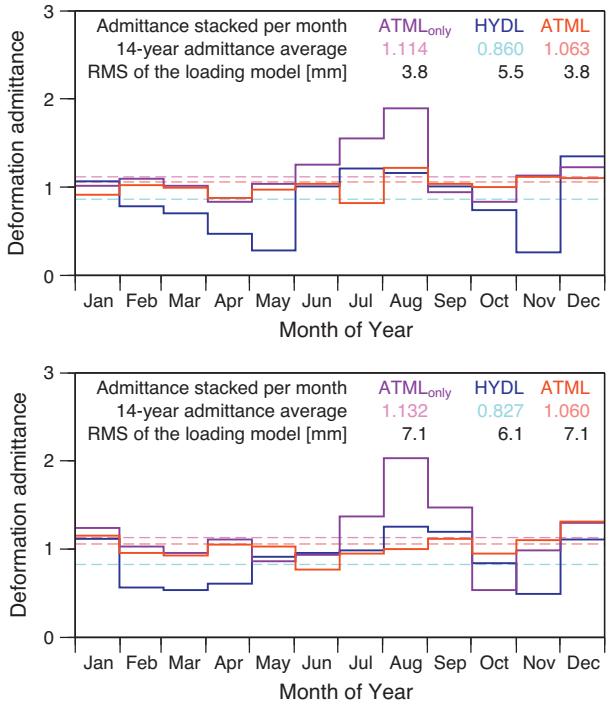

Fig. 7. Site-specific admittance factors for the vertical hydrological (HYDL) and atmospheric pressure (ATML) loading deformation. Estimates are averages for each month of the year (solid lines) and over 14 years (dashed lines). Solution types: ATML is applied only (violet), HYDL and ATML are applied commonly (blue, red). The RMS refers to the modelled vertical displacements over 14 years. Top: Zimmerwald (Switzerland, Central Europe). Bottom: Arti (Russia, Siberia).

factors were provided. Rather, in order to assess the consistency between model and observations on an annual scale, they averaged the admittance estimates for a particular month of the year from a 15-year time series. In particular for the summer months, larger deviations from the model predictions were found and attributed to remaining loading effects.

We performed an analogue analysis for the dominant vertical component. Fig. 7 shows the resulting 12 admittance factors per site for stations Zimmerwald (Switzerland) and Arti (Russia). In comparison with Fig. 6 of Dach et al. (2011), we obtain equivalent results applying only the ATML model (solution [4], Fig. 7, violet lines). Here, larger discrepancies from unity suggest a worse model performance. However, taking into account both the HYDL and ATML (solution [1]) notably reduces the scatter of the monthly ATML admittance estimates with respect to the overall mean (Fig. 7, red lines). With regards to the HYDL model, larger deviations are still present (Fig. 7, blue lines). A possible explanation is the poorer temporal resolution of the WGHM which is monthly as well.

5. Conclusions

GPS measurements are affected by changing load deformation induced by variations of surface masses. In this study, they were used to validate model-based time series of crustal deformation derived from variations of continental water storage and atmospheric pressure. Gravitational consistency and mass conservation were forced on the surface mass load models used as input. Rather than comparing site coordinate time series to corresponding model outputs we directly estimated the admittance of the displacement time series from GPS measurements.

We find promising results when applying WGHM for the continental water storage effect and the NCEP-based displacements

[3] http://gemini.gsfc.nasa.gov/aplo/Load_Love2_CM.dat.

computed by Petrov and Boy (2004) for the atmospheric pressure induced effect. Our findings confirm that deformation admittances can be determined separately for the hydrological and atmospheric loading. A worse model performance is determined for the same atmospheric pressure related displacements when ignoring the hydrological loading effect.

For Europe and North America, which have a high station density, spatially coherent patterns of admittance values are identified. The geographic distribution of areas where WGHM over- or underestimates corresponds well with large river basins for which GRACE gravity field data were compared to water storage variations as computed by WGHM. In the future, spatial coverage of the validation may be improved by evaluating additional GPS sites in South America, Africa and Asia.

Results of this study are restricted by the monthly time resolution of the WGHM. The RMS of monthly water storage variations is expected to be smaller than that of daily or subdaily values. This smoothing most probably causes a bias and systematically affects the corresponding admittance estimates. In this regard, further investigations will include a higher temporal resolution for the hydrological load representation. The global ATML admittance reveals significant differences from the applied model, too. Future attempts will include ATML-related site displacements that refer also to variations of the total atmospheric mass.

The approach of estimating the admittance of a function that depends on the load potential can be applied to other space geodetic observations, too. In particular, satellite gravimetric data allow quantifying the admittance of model-based variations in the Earth's gravitational potential field that are caused by mass transport. However, the application of GPS for validation purposes plays a unique role. Based on GPS measurements, the validity of load models can be evaluated for different sites with high (subhourly) temporal resolution. Corresponding models are applied in the GRACE data processing in order to perform a dealiasing concerning the effect of high frequency gravity field changes.

Acknowledgements

We thank the International GNSS Service (IGS, Dow et al., 2005) for providing the observation data via its data centers. Figures were generated with the Generic Mapping Tools (Wessel and Smith, 1998). Parts of the analyses were performed using the freely available software archive SHTOOLS (http://www.ipgp.fr/~wieczor/SHTOOLS/SHTOOLS.html). Part of this study was funded by the German Research Foundation under Grant DI 473/41-2 (DFG Special Priority Program SPP 1257 Mass Transport and Mass Distribution in the System Earth). We also thank two anonymous reviewers for their careful and constructive feedback.

References

Alcamo, J., Döll, P., Henrichs, T., Kaspar, F., Lehner, B., Rösch, T., Siebert, S., 2003. Development and testing of the WaterGAP 2 global model of water use and availability. Hydrol. Sci. J. 3 (48), 317–338.

Blewitt, G., 2003. Self-consistency in reference frames, geocenter definition, and surface loading of the solid Earth. J. Geophys. Res. 108 (B2).

Blewitt, G., Clarke, P., 2003. Inversion of Earth's changing shape to weigh sea level in static equilibrium with surface mass redistribution. J. Geophys. Res. 108 (B62311).

Boehm, J., Werl, B., Schuh, H., 2006. Troposphere mapping functions for GPS and very long baseline interferometry from European Centre for Medium-Range Weather Forecasts operational analysis data. J. Geophys. Res. 111 (B02406).

Clarke, P.J., Lavallée, D.A., Blewitt, G., van Dam, T.M., Wahr, J.M., 2005. Effect of gravitational consistency and mass conservation on seasonal surface mass loading models. Geophys. Res. Lett. 32 (L08306).

Dach, R., Böhm, J., Lutz, S., Steigenberger, P., Beutler, G., 2011. Evaluation of the impact of atmospheric pressure loading modeling on GNSS data analysis. J. Geodesy 85 (2), 75–91.

Dach, R., Hugentobler, U., Fridez, P., Meindl, M. (Eds.), 2007. Bernese GPS Software Version 5.0. Astronomical Institute, University of Bern, Switzerland.

Dahlen, F.A., 1976. The passive influence of the oceans upon the rotation of the Earth. Geophys. J. R. Astron. Soc. 46, 363–406.

Davis, J.L., Elósegui, P., Mitrovica, J.X., Tamisiea, M.E., 2004. Climate-driven deformation of the solid Earth from GRACE and GPS. Geophys. Res. Lett. 31 (L24605).

Döll, P., Kaspar, F., Lehner, B., 2003. A global hydrological model for deriving water availability indicators: model tuning and validation. J. Hydrol. 270, 105–134.

Dow, J.M., Neilan, R.E., Gendt, G., 2005. The International GPS Service (IGS): celebrating the 10th anniversary and looking to the next decade. Adv. Space Res. 36 (3), 320–326.

Farrel, W.E., Clark, J.A., 1976. On postglacial sea level. Geophys. J. R. Astron. Soc. 46 (3), 647–667.

Farrell, W.E., 1972. Deformation of the Earth by surface loads. Rev. Geophys. Space Phys. 10 (3), 761–797.

Fritsche, M., Dietrich, R., Rülke, A., Rothacher, M., Steigenberger, P., 2009. Low-degree earth deformation from reprocessed GPS observations. GPS Solut. 14 (2), 165–175.

Güntner, A., Stuck, J., Werth, S., Döll, P., Verzano, K., Merz, B., 2007. A global analysis of temporal and spatial variations in continental water storage. Water Resour. Res. 43 (W05416).

Hunger, M., Döll, P., 2008. Value of river discharge data for global-scale hydrological modeling. Hydrol. Earth Syst. Sci. 12, 841–861.

Kaniuth, K., Vetter, S., 2005. Estimating atmospheric pressure loading regression coefficients from GPS observations. GPS Solut. 10 (2), 126–134.

MacMillan, D.S., Gipson, J.M., 1994. Atmospheric pressure loading parameters from very long baseline interferometry observations. J. Geophys. Res. 99 (B9), 18081–18087.

Pagiatakis, S.D., 1990. The response of a realistic earth to ocean tide loading. GJI 103 (2), 541–560.

Petrov, L., Boy, J.-P., 2004. Study of the atmospheric pressure loading signal in very long baseline interferometry observations. J. Geophys. Res. 109 (B03405).

Ponte, R.M., Ray, R.D., 2002. Atmospheric pressure corrections in geodesy and oceanography: a strategy for handling air tides. Geophys. Res. Lett. 29 (24), 2153.

Rudolf, B., Schneider, U., 2005. Calculation of gridded precipitation data for the global land surface using in-situ gauge observations. In: Proceedings of the 2nd Workshop of the 46 International Precipitation Working Group (IPWG), Monterey, October 2004. pp. 231–247, http://gpcc.dwd.de.

Rülke, A., Dietrich, R., Fritsche, M., Rothacher, M., Steigenberger, P., 2008. Realization of the terrestrial reference system by a reprocessed global GPS network. J. Geophys. Res. 113 (B08403).

Schmidt, R., Petrovic, S., Güntner, A., Barthelmes, F., Wünsch, J., Kusche, J., 2008. Periodic components of water storage changes from GRACE and global hydrological models. J. Geophys. Res. 113 (B08419).

Steigenberger, P., Boehm, J., Tesmer, V., 2009. Comparison of GMF/GPT with VMF1/ECMWF and implications for atmospheric loading. J. Geodesy 83 (10), 943–951.

Steigenberger, P., Rothacher, M., Dietrich, R., Fritsche, M., Rülke, A., Vey, S., 2006. Reprocessing of a global GPS network. J. Geophys. Res. 111 (B05402).

Tregoning, P., Herring, T.A., 2006. Impact of a priori zenith hydrostatic delay errors on GPS estimates of station heights and zenith total delays. Geophys. Res. Lett. 33 (L23303).

Tregoning, P., van Dam, T., 2005. Atmospheric pressure loading corrections applied to GPS data at the observation level. Geophys. Res. Lett. 32 (L22310).

Tregoning, P., Watson, C., 2009. Atmospheric effects and spurious signals in GPS analyses. J. Geophys. Res. 114 (B09403).

Trenberth, K.E., Smith, L., 2005. The mass of the atmosphere: a constraint on global analyses. J. Climate 18 (6), 864–875.

van Dam, T., Wahr, J., Lavallée, D., 2007. A comparison of annual vertical crustal displacements from GPS and Gravity Recovery and Climate Experiment (GRACE) over Europe. J. Geophys. Res. 112 (B03404).

van Dam, T.M., Blewitt, G., Heflin, M.B., 1994. Atmospheric pressure loading effects on Global Positioning System coordinate determinations. J. Geophys. Res. 99 (B12), 23939–23950.

van Dam, T.M., Herring, T.A., 1994. Detection of atmospheric pressure loading using very long baseline interferometry measurements. J. Geophys. Res. 99 (B3), 4505–4517.

Werth, S., Güntner, A., 2010. Calibration analysis for water storage variability of the global hydrological model WGHM. HESS 14, 59–78.

Wessel, P., Smith, W.H.F., 1998. New, improved version of the Generic Mapping Tools released. EOS Trans. AGU 79.